Jack C. Heberlig
NASA TN D-628

NASA TN D-628

EXTRA COPY

TECHNICAL NOTE

D-628

LANDING CHARACTERISTICS OF A REENTRY CAPSULE WITH A TORUS-SHAPED AIR BAG FOR LOAD ALLEVIATION

By John R. McGehee and Melvin E. Hathaway

Langley Research Center
Langley Field, Va.

NATIONAL AERONAUTICS AND SPACE ADMINISTRATION
WASHINGTON November 1960

NATIONAL AERONAUTICS AND SPACE ADMINISTRATION

TECHNICAL NOTE D-628

LANDING CHARACTERISTICS OF A REENTRY CAPSULE WITH A TORUS-SHAPED AIR BAG FOR LOAD ALLEVIATION

By John R. McGehee and Melvin E. Hathaway

SUMMARY

An experimental investigation has been made to determine the landing characteristics of a conical-shaped reentry capsule by using torus-shaped air bags for impact-load alleviation. An impact bag was attached below the large end of the capsule to absorb initial impact loads and a second bag was attached around the canister to absorb loads resulting from impact on the canister when the capsule overturned. A 1/6-scale dynamic model of the configuration was tested for nominal flight paths of 60° and 90° (vertical), a range of contact attitudes from -25° to 30°, and a vertical contact velocity of 12.25 feet per second. Accelerations were measured along the X-axis (roll) and Z-axis (yaw) by accelerometers rigidly installed at the center of gravity of the model. Actual flight paths, contact attitudes, and motions were determined from high-speed motion pictures. Landings were made on concrete and on water.

The peak accelerations along the X-axis for landings on concrete were in the order of 30g for a 0° contact attitude. A horizontal velocity of 7 feet per second, corresponding to a flight path of 60°, had very little effect upon the peak accelerations obtained for landings on concrete. For contact attitudes of -25° and 30° the peak accelerations along the Z-axis were about ±15g, respectively. The peak accelerations measured for the water landings were about one-third lower than the peak accelerations measured for the landings on concrete.

Assuming a rigid body, computations were made by using Newton's second law of motion and the force-stroke characteristics of the air bag to determine accelerations for a flight path of 90° (vertical) and a contact attitude of 0°. The computed and experimental peak accelerations and strokes at peak acceleration were in good agreement for the model. The special scaling appears to be applicable for predicting full-scale time and stroke at peak acceleration for a landing on concrete from a 90° flight path at a 0° attitude. It appears that the full-scale configuration would have adequate stroke to develop peak accelerations approximately the same as those obtained from the model for the range of attitudes and flight paths investigated.

INTRODUCTION

There has been considerable interest shown in methods for alleviating the landing loads of space capsules when the landing may occur on the ground or in the water. One method for reducing these loads involves the use of air bags. Some full-scale research has been conducted on the use of air bags for reducing the landing loads of air-dropped cargo, but from literature available it appears that this work has been limited in range of flight paths and contact attitudes.

L
7
9
2

The present investigation was conducted to determine the landing characteristics of a conical-shaped reentry capsule with torus-shaped air bags for impact-load alleviation. The 1/6-scale-model capsule configuration is shown in figure 1. This dynamic model was landed on concrete and on water. An impact bag was attached below the large end of the capsule to absorb initial impact loads and a second bag was attached around the canister to absorb loads resulting from impact on the canister when the capsule overturned. The experimental investigations were conducted for two nominal flight paths and a range of contact attitudes to simulate some of the possible flight paths and impact attitudes that might occur with a parachute letdown.

Assuming the capsule to be a rigid body, computations were made to determine the loads imposed upon the configuration for a landing on concrete. The equations, from which the computations were made, were based upon Newton's second law of motion and the force-stroke characteristics of the air bag. The calculations were made for an earth landing. These investigations were made in the Pliant Structures Branch of the Langley Research Center.

SYMBOLS

A	area, sq ft
C	orifice discharge coefficient
D	diameter of torus, ft
F	force developed by air bag during landing, lb
g	acceleration due to gravity, 32.2 ft/sec^2
I	mass moment of inertia, slug-ft^2
l	geometric length, ft

M	mass of configuration, slug
m	mass of air, slug
Δm	differential mass of air, slug
p	pressure, lb/sq ft
r	section radius of torus, ft
t	time from instant of contact, sec
Δt	differential time, sec
V	volume in air bag, cu ft
W	weight, lb
x	stroke (measured vertically for all attitudes), ft
$\dot{x}$	velocity, $\frac{dx}{dt}$, ft/sec
$\ddot{x}$	acceleration, $\frac{d^2x}{dt^2}$, ft/sec^2
Δx	differential stroke, ft
ρ	mass density of air at standard conditions (0.002378 slug/cu ft)

Subscripts:

a	atmospheric
b	blowout
c	contact
e	escaped
f	footprint (area of bag in contact with ground)
i	initial
o	orifice

L 7 9 2

t	time after contact
t-Δt	from previous step in step-by-step computation

APPARATUS AND PROCEDURE

A drawing of the capsule configuration is shown in figure 1. The orientation of axes, flight path, contact attitudes and force directions investigated are shown in figure 2. Pertinent dimensions, measured moments of inertia, velocity, and pressures are listed in table I.

L
7
9
2

Description of Model

The 1/6-scale dynamic-capsule model was constructed of fiberglass and plastic; the construction was as rigid as possible to reduce structural vibrations. The impact air bag was made of two layers of latex impregnated silk. The warp of the second layer of silk was rotated 90° to the warp of the first layer to reduce stretching. To accommodate landing attitudes other than 0°, the air bag was compartmented to insure adequate pressure buildup under that portion of the capsule which would make first contact in a landing.

To prevent rebound, pressure relief was required. Therefore, the air bag was divided into eight compartments and each compartment had a 3/4-inch-diameter orifice with a blowout patch. Details of the torus-shaped impact air bag are shown in figure 3. The blowout patches were constructed of the same material as the bag and consisted of three disks glued together as shown in figure 3(c). All of the tests of this investigation were made with the 15/16-inch-diameter disk installed inside the bag (see fig. 3(c)), which resulted in a blowout pressure of approximately 1 lb/sq in. gage. Details of the canister air bag are shown in figure 4. The canister air bag was made of the same material as the impact air bag but there were no inside partitions and there were only three pressure-relief orifices. These orifices were 1/2 inch in diameter and were plugged with blowout patches as shown in figure 4(c). The 5/8-inch-diameter disks were installed inside the bag. (See fig. 4(c).)

A photograph of the model with the two air bags is shown in figure 5. For the air bag to provide sufficient force to prevent the capsule from impacting the floor through the air bag, it was necessary to use an experimentally determined initial pressure of 0.25 lb/sq in. gage. The initial pressures of the bags were measured by the use of a water-filled manometer.

The instrumentation consisted of two strain-gage-type accelerometers and a strain-gage-type pressure pickup. The accelerometers were located

at the center of gravity and rigidly attached to the bottom of the model. The accelerometers were capable of measuring 200g and 25g along the X-axis and Z-axis, respectively. The natural frequency of the 200g accelerometer was about 900 cycles per second and the natural frequency of the 25g accelerometer was about 350 cycles per second. The accelerometers were damped to 65 percent of critical damping. The response of the recording equipment was flat to about 2,200 cycles per second. The pressure pickup was installed with the pressure-sensitive diaphragm located in the compartment of the torus which for attitudes different from zero was oriented to make initial contact with the landing surface. The pressure pickup was capable of measuring ±7.5 lb/sq in. gage and had a natural frequency of approximately 7,500 cycles per second. The pressure pickup was undamped but the response was limited to about 65 cycles per second by the recording equipment.

L
7
9
2

Test Methods

The tests for the 90° (vertical) flight path were made by a free-fall method where the model was dropped from the height required to obtain, under the influence of gravitational acceleration, a vertical velocity of 12.25 feet per second at contact. The tests for the nominal 60° flight path were conducted by releasing the model from a pendulum as shown in the sketch of figure 6. This test procedure is discussed in detail in reference 1. A range of contact attitudes from -25° to 30° was investigated for both flight paths. (See fig. 2.) The contact attitudes, flight paths, and motions of the capsule were recorded by a high-speed motion-picture camera. Landings were made on concrete and on water. The landings on concrete were made on a very smooth concrete floor. Water landings were made in a long tank of water 6 feet deep and 18 feet wide. The investigations were made at prevailing atmospheric conditions.

Computations

An analysis of a reentry-capsule landing from a 90° (vertical) flight path at a 0° contact attitude with a torus-shaped air bag for load alleviation was made by utilizing Newton's second law of motion and the force-stroke characteristics of the air bag. For the purpose of this analysis, the following assumptions were made: (1) parachute release occurred at contact and the only force causing deceleration was the gas-pressure force, (2) the air bag was inelastic and flexible, and (3) the orifice discharge coefficient was 0.6. An analytical study of soft landings is presented in reference 1 for vertical and horizontal cylinders and spherical and hemispherical gas bags.

The decelerating force at any time after contact is equal to the product of the footprint area of the bag and the pressure in the bag:

$$F_t = A_{f,t} P_{t,gage} \tag{1}$$

where the footprint area of the bag, as a function of the stroke (see fig. 7), was derived from the geometry of the bag. The footprint area of the bag may be computed from the following equation:

$$A_{f,t} = \pi D \sqrt{4rx_t - x_t^2} \tag{2}$$

The gage pressure in the air bag at any time after contact may be determined from the pressure-volume relation and air-mass ratios when isothermal compression and expansion are assumed:

$$P_{t,gage} = \left[\left(\frac{P_i V_i}{V_t} \right) \left(\frac{m_i - m_{e,t}}{m_i} \right) - P_a \right] \tag{3}$$

where the mass of air escaping (m_e) is zero until the orifices open.

The volume in the bag at any time after contact (see fig. 7) may be computed from the following equation:

$$V_t = V_i - \sum A_{f,t} \Delta x \tag{4}$$

where $\sum A_{f,t} \Delta x$ represents the volume change due to compression. The volume defined by the term $\sum A_{f,t} \Delta x$ is not exact, but is a simplification which results in fair agreement between computed and experimental maximum accelerations. Curves of footprint area $(A_{f,t})$ and volume (V_t) at any time after contact as a function of stroke are shown in a dimensionless form in figure 8.

After the orifices open, the mass of air escaping through the orifices $(m_{e,t})$ may be determined from the following equation:

$$m_{e,t} = \sum \Delta m_{e,t} = \sum \rho_t C A_o \Delta t \sqrt{\frac{2P_a}{\rho_t} \left(\frac{P_{t-\Delta t}}{P_a} - 1 \right)} \tag{5}$$

The decelerating force at any time after contact may now be rewritten in the following form:

$$F_t = \pi D\sqrt{4rx_t - x_t^2}\left[\left(\frac{P_i V_i}{V_t}\right)\left(\frac{m_i - m_{e,t}}{m_i}\right) - P_a\right] \qquad (6)$$

Employing the above equation the accelerations were calculated using a step-by-step process similar to the procedure used in reference 2.

Scaling

Scaling laws used in the testing of dynamic models require that pressure and stroke vary as the scale factor, and that time and velocity vary as the square root of the scale factor. Because the atmospheric pressure was not scaled in the present investigation, special scaling is required to predict full-scale maximum acceleration and the stroke, velocity, and time at which maximum acceleration occurs. The special scaling was established by using the computational procedure previously discussed to predict full-scale accelerations from which the appropriate scaling factors were empirically determined. Computations were made only for a flight path of 90° and a contact attitude of 0°. This computational procedure is not applicable to other conditions; also, the scaling procedure does not permit continuous scaling throughout an impact. The factors presented in the following table were determined when peak accelerations were the same for model and full-scale configurations.

Quantity	Model scale	Scale factor, $\lambda = 6$	Full scale
Area	A	λ^2	$\lambda^2 A$
Force	F	λ^3	$\lambda^3 F$
Inertia	I	λ^5	$\lambda^5 I$
Geometric length	l	λ	λ^l
Mass	M	λ^3	$\lambda^3 M$
Volume	V	λ^3	$\lambda^3 V$
Weight	W	λ^3	$\lambda^3 W$
Contact velocity	$\dot{x}_c$	$\lambda^{0.5}$	$\lambda^{0.5}\dot{x}_c$
Acceleration	$\ddot{x}$	1	$\ddot{x}$
Initial gage pressure	p_i	λ	λp_i
Blowout gage pressure	p_b	λ	λp_b
Atmospheric pressure	p_a	1	p_a

The following parameters require special scaling because the atmospheric pressure was the same for the model and the full-scale configuration.

Quantity	Model scale	Scale factor, $\lambda = 6$	Full scale
Time	t	$\lambda^{0.73}$	$\lambda^{0.73}t$
Stroke	x	$\lambda^{1.23}$	$\lambda^{1.23}x$
Velocity during impact	$\dot{x}$	$\lambda^{0.35}$	$\lambda^{0.35}\dot{x}$

The preceding special scaling is only rigorously valid for predicting peak accelerations and the stroke, velocity, and time at peak acceleration for the contact velocity, orifice size, and configuration weight presented in this paper. For large variations in contact velocity, orifice size, and weight, it is recommended that the scale factors for the quantities requiring special scaling be reevaluated.

RESULTS AND DISCUSSION

Presentation of Experimental Results

Typical time histories of accelerations and stroke are shown in figures 9, 10, and 11 for landings on concrete. Typical oscillograph records of accelerations and air-bag pressure are shown in figure 12. Peak accelerations along the X-axis, from data such as those presented in figure 9, are shown plotted in figure 13 as a function of contact attitude with flight-path angle as a parameter. Data are presented for drops made on concrete and on water. For landings on concrete, the peak accelerations along the X-axis occurred at a contact attitude of 0° and were of the order of 30g. At contact attitudes of approximately -25° and 30°, the peak accelerations were about 22g. It is interesting to note that a horizontal velocity of 7 feet per second, which corresponds to a flight path of 60°, had very little effect on the peak accelerations obtained from landings on concrete. It also may be seen in figures 9 and 11 that this horizontal velocity had very little effect on the rate of application of acceleration or the magnitude of the stroke.

The variation in the peak acceleration shown in figure 13 for the 90° flight path and 0° contact attitude may have resulted from changes in the pressure at which the patches were blown. A lower blowout pressure would result in a lower peak pressure and consequently a lower peak acceleration. This would apply until the stroke became large

enough to allow the capsule to contact the concrete before dissipation of the kinetic energy. As may be seen from figure 11, the maximum stroke obtained was approximately one-half of the stroke available with air bag tested in this investigation. The peak accelerations determined from the landings made on water were about one-third lower than those obtained from the landings made on concrete (fig. 13).

Peak accelerations along the Z-axis, from data such as those shown in figure 10, are plotted in figure 14 as a function of contact attitude with flight-path angle as a parameter. There were no appreciable accelerations along the Z-axis for a contact attitude of 0°. For increase in contact attitude, in either the positive or negative direction from 0° attitude, the peak accelerations increased. For contact attitudes of -25° and 30°, the peak accelerations along the Z-axis were about $\pm 15g$, respectively. The peak accelerations for the water landings were about one-third lower than those obtained from the landings on concrete.

Sequence photographs of landings made on concrete are shown in figure 15 for a 90° flight path and a 0° contact attitude and in figure 16 for a 63° flight path and a -26° contact attitude. As shown in figure 16, the landings made from a nominal 60° flight path resulted in rotation of the capsule after contact and a subsequent canister impact. For a landing from a nominal 60° flight path with a -25° contact attitude, a canister impact without the air bag resulted in peak accelerations along the X-axis of the order of 60g and along the Z-axis of the order of 30g. With the small air bag around the canister, the peak accelerations were approximately 2g along the X-axis and approximately 6g along the Z-axis. The large reduction in peak acceleration along the X-axis may be attributed to both the load alleviation of the small air bag and the fact that the model slid across the concrete on the canister air bag and consequently the capsule had a small acceleration applied for a long period of time. The reduction in acceleration along the Z-axis from 30g to 6g indicates the effectiveness of the small air bag in load alleviation. The model capsule was not scaled structurally, hence does not indicate the load alleviation which would probably occur on a full-scale capsule due to crushing of the canister.

Prediction of Full-Scale Results

A comparison of experimental and computed time histories of acceleration along the X-axis for a 90° flight path and a 0° contact attitude is shown in figure 17. Good agreement was obtained between computed and experimental peak accelerations and times to peak acceleration for the model. The differences between computed and experimental acceleration-time histories for the model may be attributed to change in volume of

the air bag caused by stretching, loss of pressure due to leakage, and differences between computed and experimental footprint areas.

The full-scale acceleration-time history shown (dashed line, fig. 17) was computed using parameters defined by the special scaling previously discussed. The computed model-scale data transformed to full scale by the special scaling is shown by the curve coded with a long dash and two short dashes. The solid line shown on figure 17 represents the experimental data scaled to full size by applying the scaling laws for dynamic-model tests; a comparison between this curve and the computed full-scale curve indicates a time discrepancy. This discrepancy is a result of conducting the model tests at atmospheric pressure rather than at scaled atmospheric pressure.

Experimental and computed stroke-time histories for a flight path of 90° (vertical) and a contact attitude of 0° are shown in figure 18. Fair agreement was obtained between the computed and experimental model strokes. The computed full-scale stroke (dashed line) and the computed model-scale stroke transformed to full scale by the special scaling (long dash and two short dashes) are also shown on figure 18. The solid line shown represents the full-scale stroke obtained by applying the normal scaling laws for dynamic-model tests to the experimental model stroke. The computed full-scale stroke is about 20 percent greater than the model stroke scaled by the scaling laws for dynamic-model tests. This difference results from testing the model at atmospheric pressure rather than at scaled atmospheric pressure. The computed full-scale stroke is about 40 percent of the stroke available with the bag design considered; from figure 11, it may be seen that the maximum stroke in the model tests, regardless of flight-path angle or contact attitude, was less than 50 percent of the stroke available. Therefore, it appears that a full-scale configuration would have adequate stroke to develop peak accelerations approximately the same as those obtained from the model test. Because the configuration presented in this report was not an optimum design, it should be emphasized that a design for a specific configuration should use greater than 50 percent of the available stroke to increase load-alleviating-system efficiency.

CONCLUDING REMARKS

Experimental and analytical investigations have been made to determine the landing characteristics of a conical-shaped reentry capsule using a torus-shaped air bag for load alleviation. It was found that a horizontal velocity of 7 feet per second, which corresponds to a 60° flight path, had very little effect upon the peak accelerations obtained for landings on concrete. The peak accelerations along the X-axis for a landing on concrete were in the order of 30g for a

0° contact attitude. Changes in contact attitude to -25° or 30° reduced the peak accelerations to about 22g. There were no appreciable accelerations along the Z-axis for a contact attitude of 0°. For contact attitudes of -25° and 30° the peak accelerations along the Z-axis were about $\pm$15g, respectively. The accelerations measured for the water landings were about one-third lower than those measured for the landings on concrete.

The computed and experimental peak accelerations and strokes at peak acceleration were in good agreement for the model. The special scaling appears to be applicable for predicting full-scale time and stroke at peak acceleration for a landing on concrete from a 90° flight path at a 0° attitude. It appears that the full-scale configuration would have adequate stroke to develop peak accelerations approximately the same as those obtained from the model test for the range of attitudes and flight paths investigated.

Langley Research Center,
National Aeronautics and Space Administration,
Langley Field, Va., September 8, 1960.

REFERENCES

1. Esgar, Jack B., and Morgan, William C.: Analytical Study of Soft Landings on Gas-Filled Bags. NASA TR R-75, 1960.

2. McGehee, John R., Hathaway, Melvin E., and Vaughan, Victor L., Jr.: Water-Landing Characteristics of a Reentry Capsule. NASA MEMO 5-23-59L, 1959.

TABLE I

PERTINENT VALUES FOR THE REENTRY CAPSULE AND IMPACT BAG

	1/6-scale model	Full scale
Configuration weight, lb	5.55	1,200
Height (overall), ft	1.79	10.75
Maximum diameter of capsule, ft	1.04	6.25
Center-of-gravity location from maximum diameter, ft	0.21	1.28
Rolling moment of inertia, slug-ft^2	0.017	132
Pitching moment of inertia, slug-ft^2	0.040	311
Yawing moment of inertia, slug-ft^2	0.040	311
Maximum diameter of impact bag, ft	1.33	8.00
Section diameter of impact bag, ft	0.58	3.50
Maximum diameter of canister bag, ft	0.75	4.50
Section diameter of canister bag, ft	0.17	1.00
Orifice diameter (impact bag), ft	0.06	0.38
Orifice diameter (canister bag), ft	0.04	0.25
Initial pressure in bag, lb/sq in. gage	0.25	1.5
Relief pressure of impact bag, lb/sq in. gage	approx. 1.0	approx. 6.0
Atmospheric pressure, psi	14.7	14.7
Vertical velocity at contact, fps	12.25	30.00

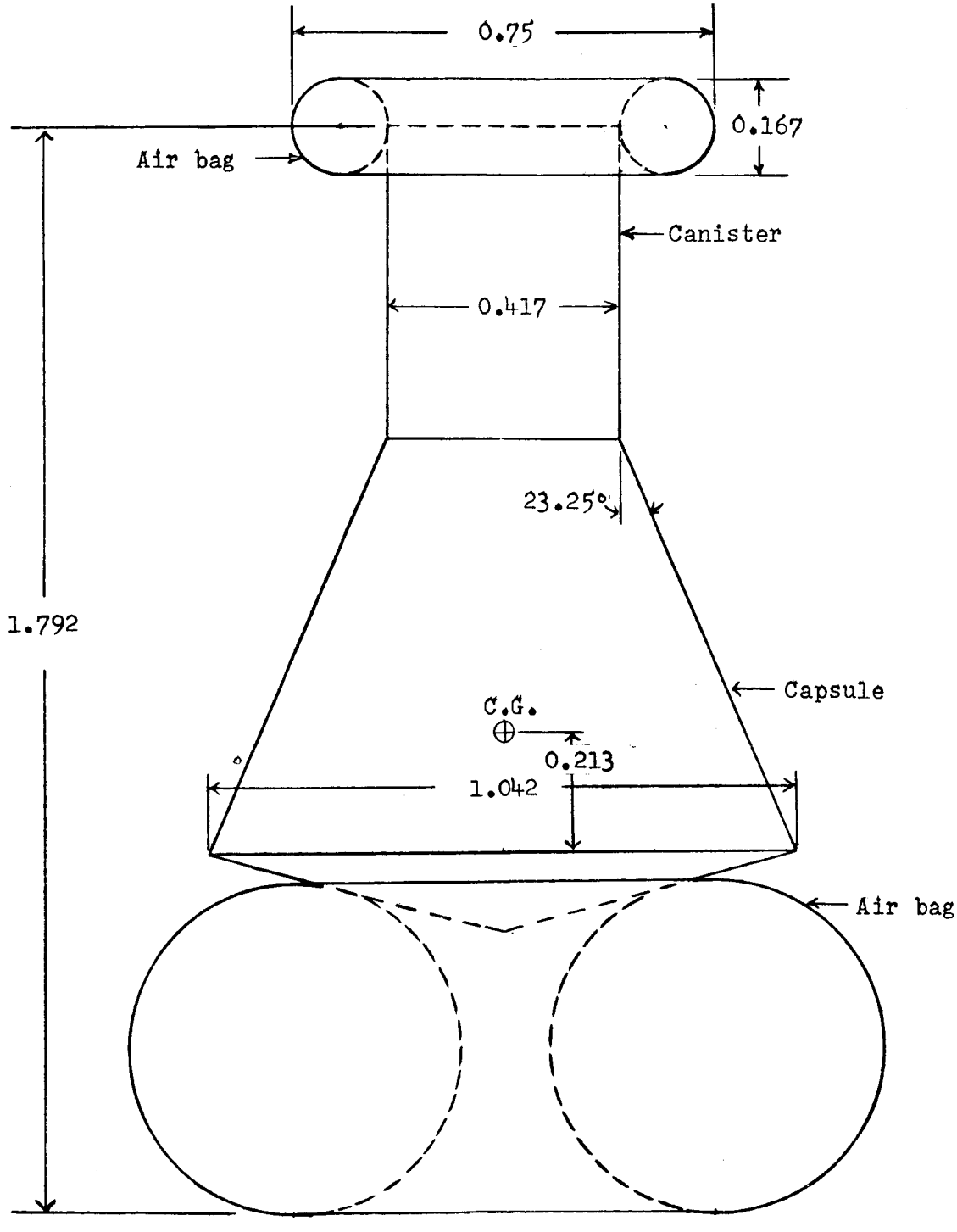

Figure 1.- Capsule configuration. All dimensions are in feet model scale.

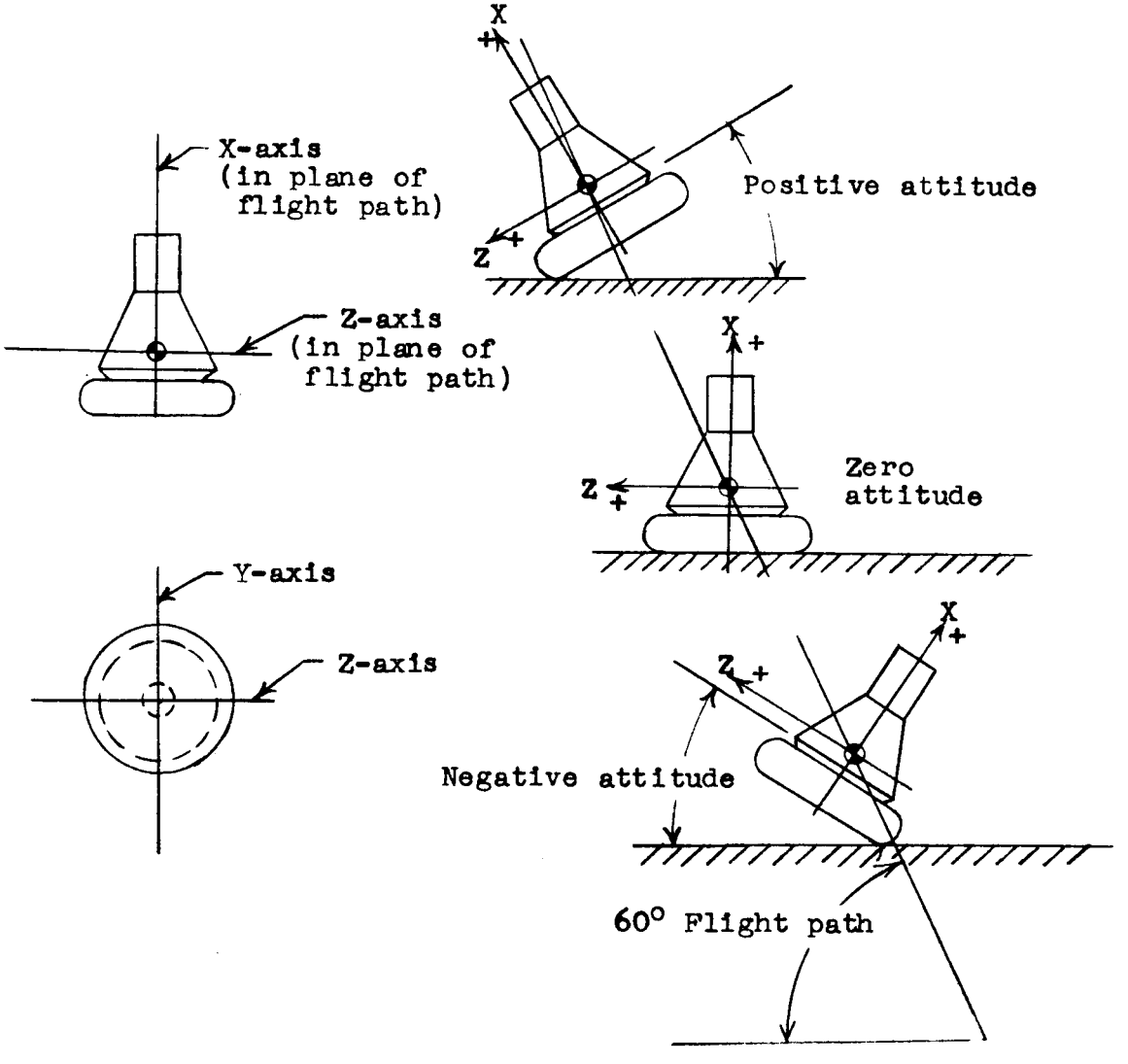

Figure 2.- Sketches identifying axes, flight paths, contact attitudes, and force directions.

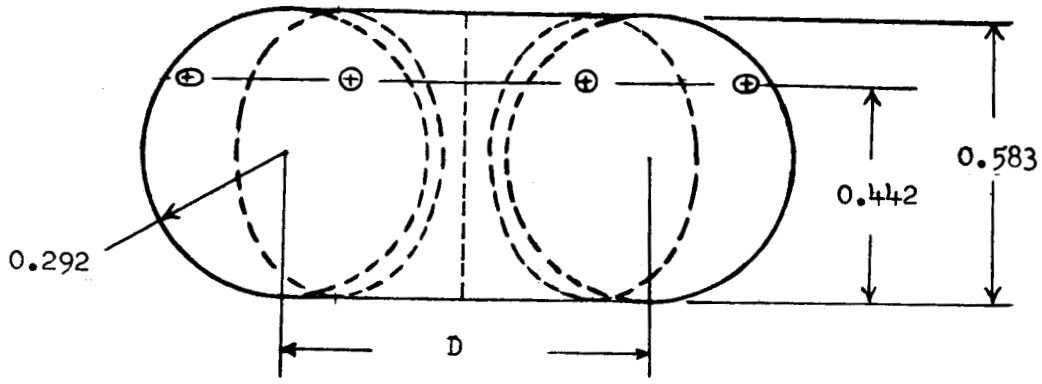

(a) Side view.

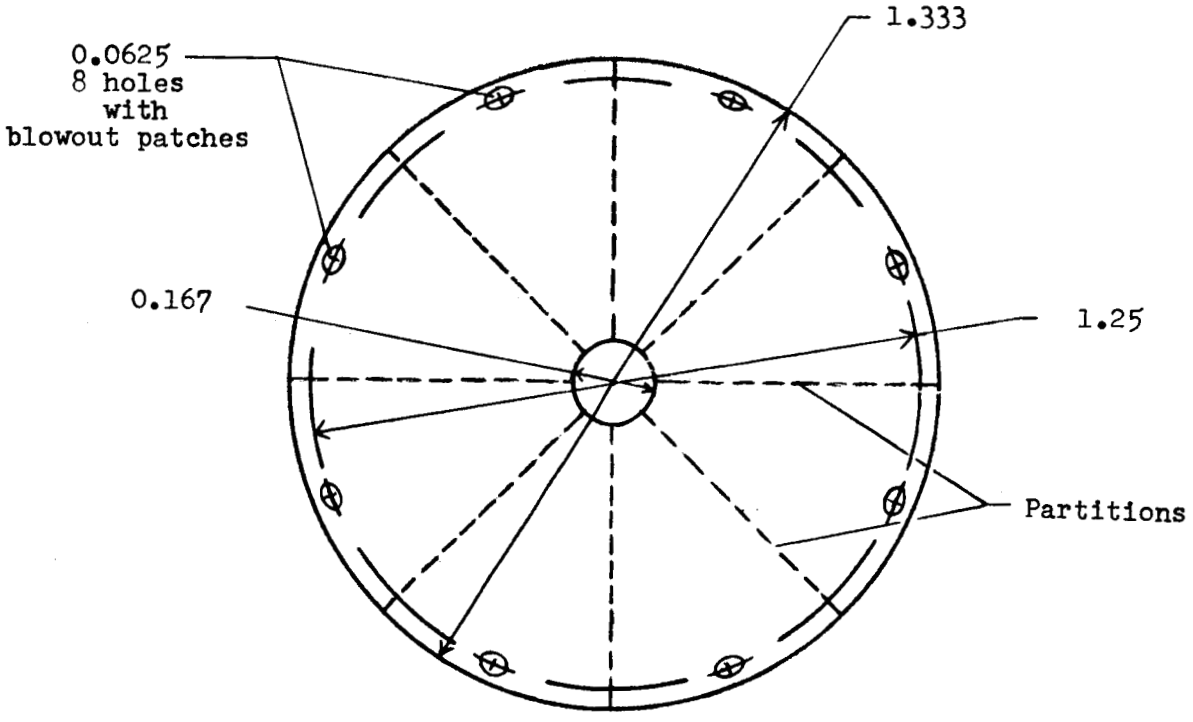

(b) Top view.

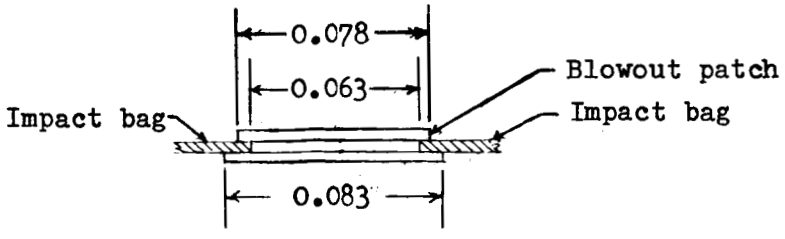

(c) Section through blowout patch.

Figure 3.- Details of torus-shaped impact air bag. All dimensions are in feet model scale.

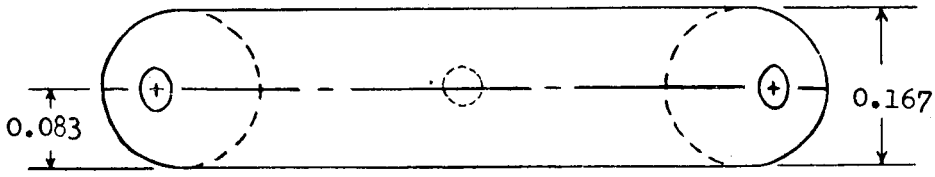

(a) Side view.

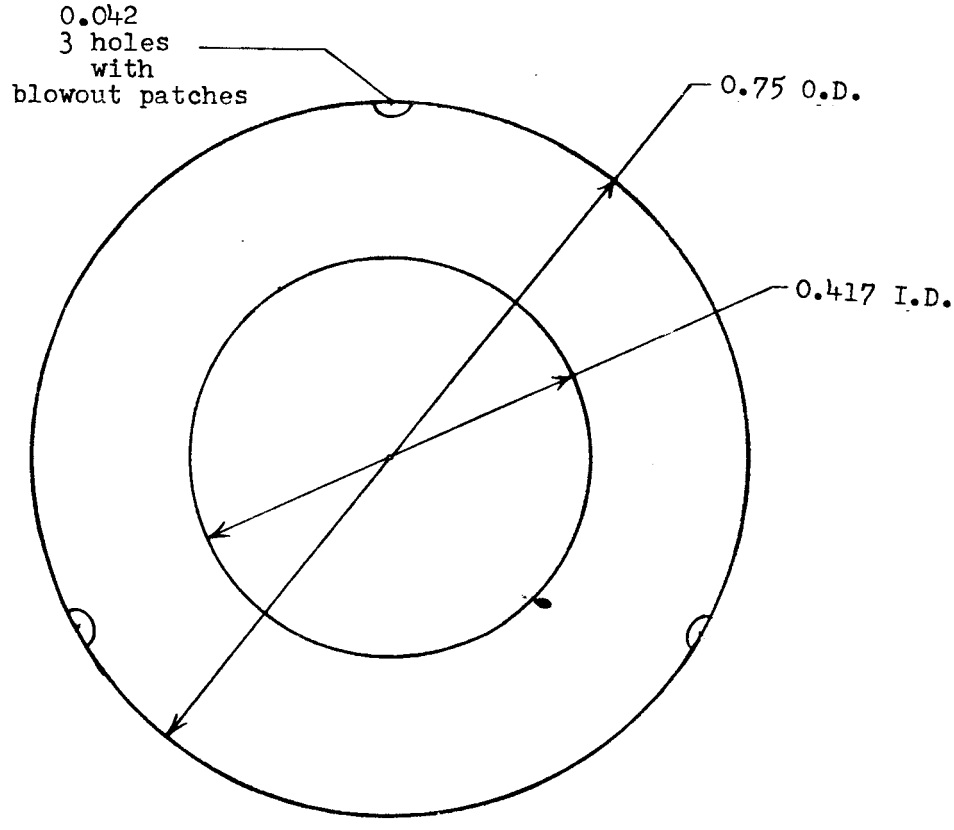

(b) Top view.

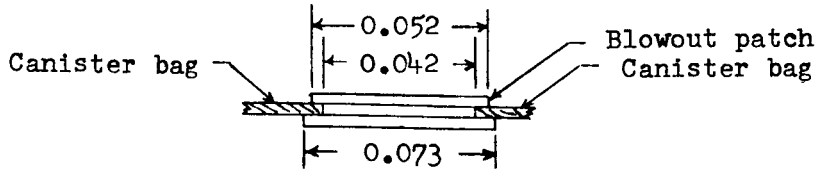

(c) Section through blowout patch.

Figure 4.- Details of torus-shaped canister air bag. All dimensions are in feet model scale.

L-60-5542

Figure 5.- Photograph of model with two impact bags.

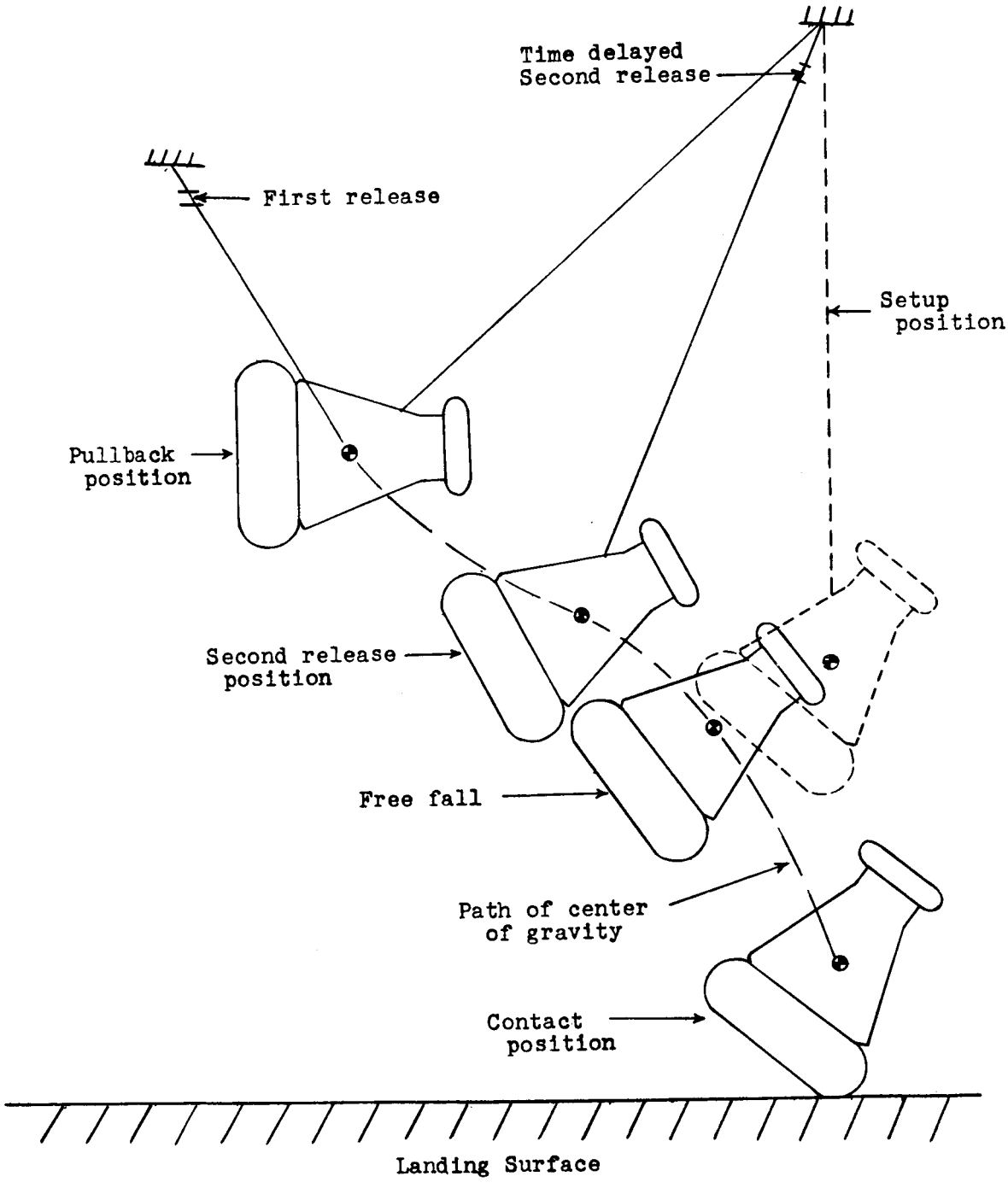

Figure 6.- Sketch illustrating the pendulum method employed for obtaining 60° flight path.

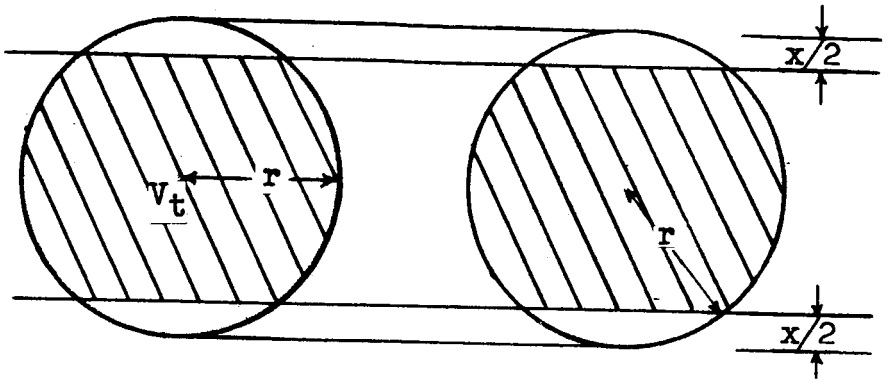

Section A-A

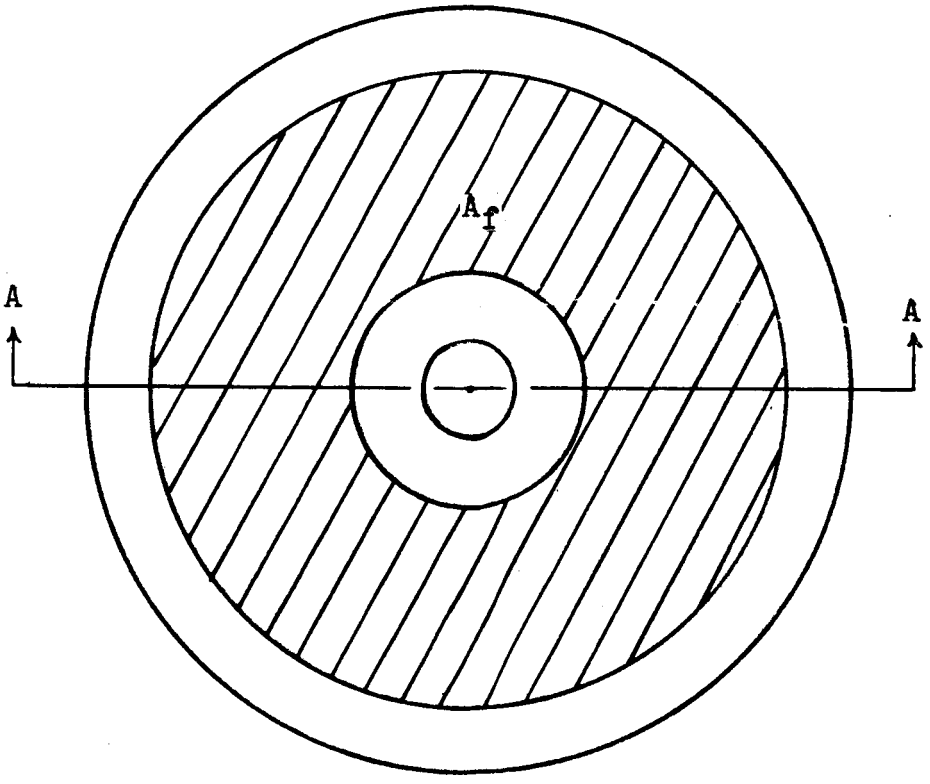

Figure 7.- Sketch defining footprint area and volume as a function of stroke.

L-792

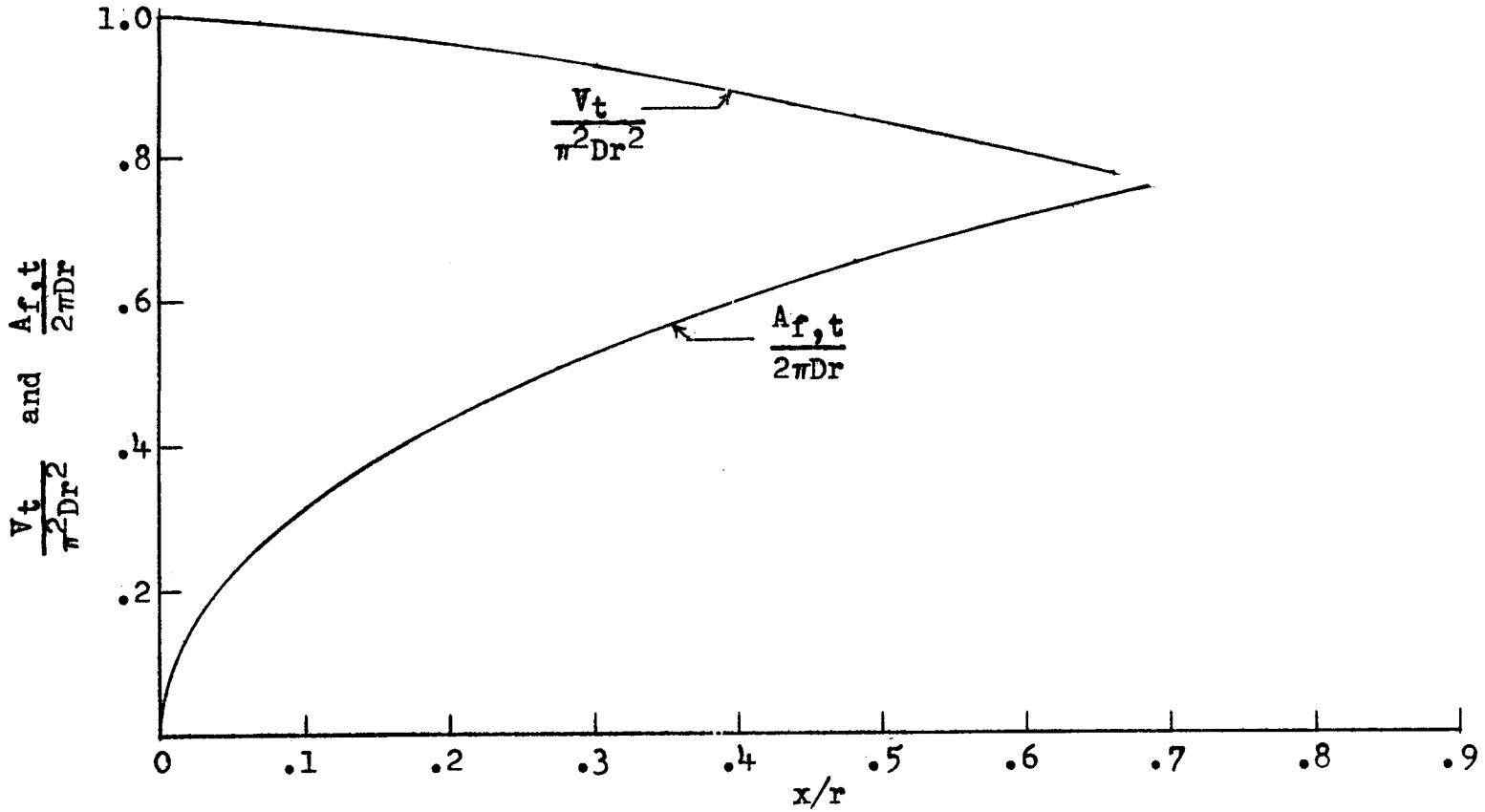

Figure 8.- Footprint area and volume in impact bag at any time after contact as a function of stroke.

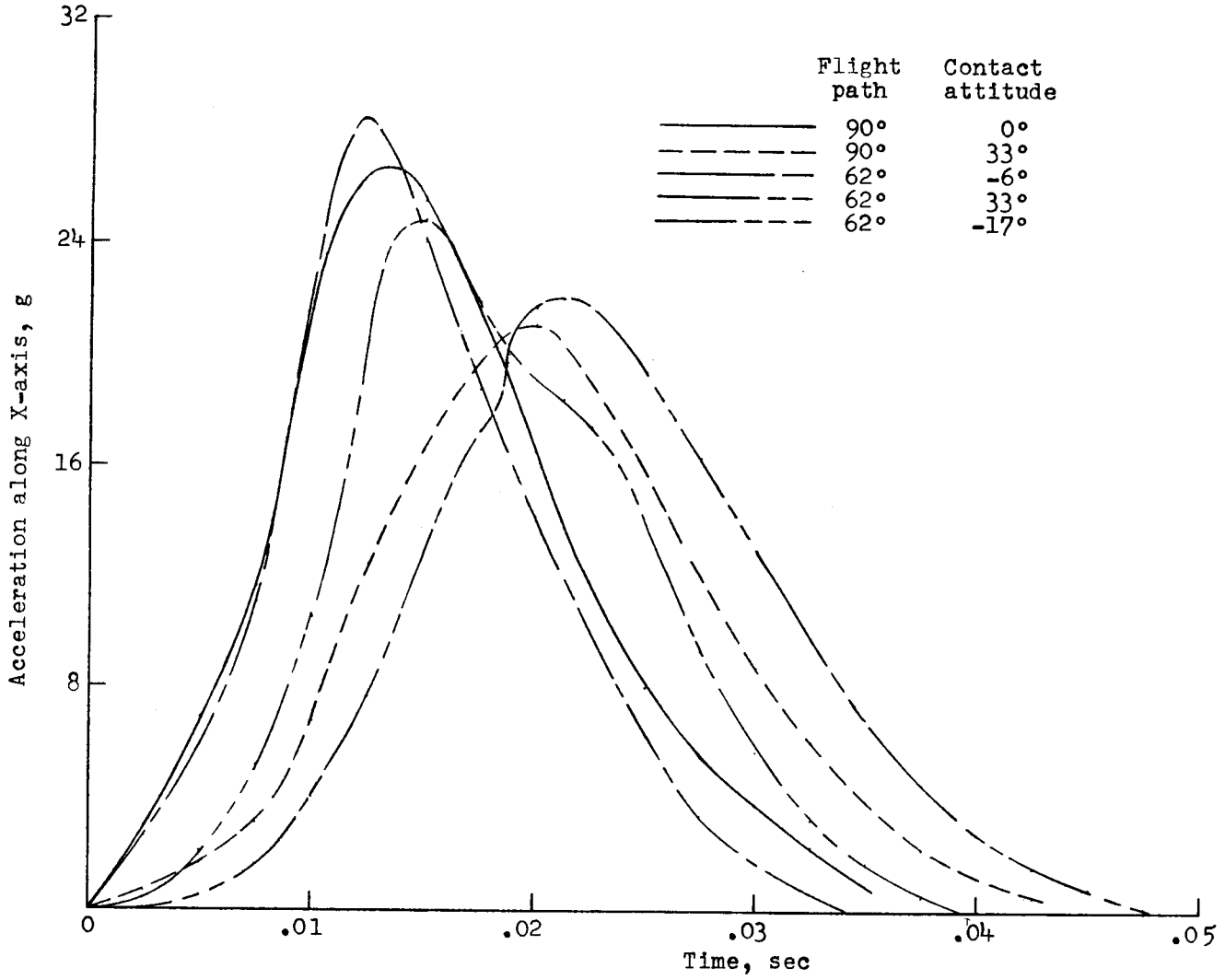

Figure 9.- Typical acceleration-time histories for accelerations measured along the X-axis. All values are model scale.

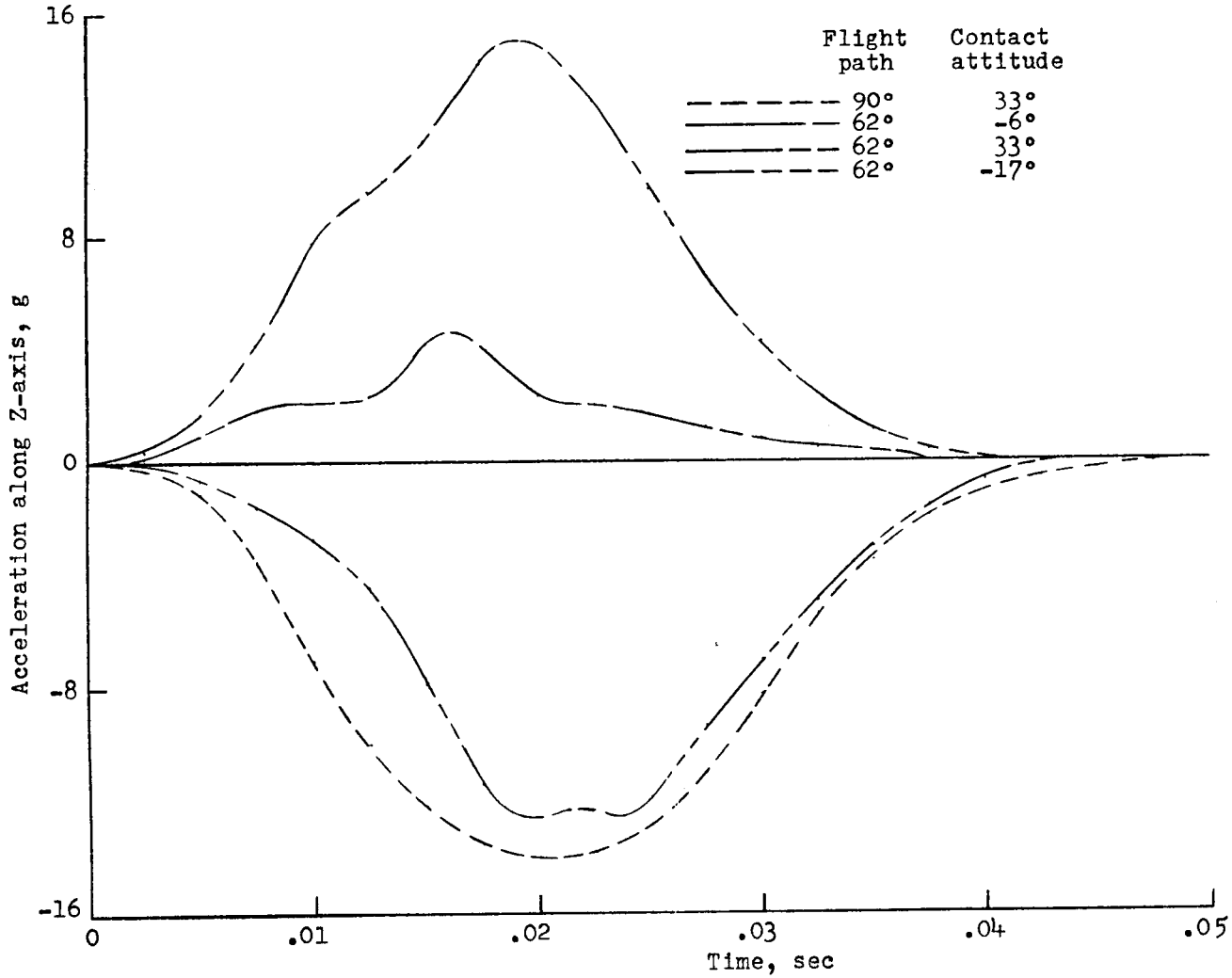

Figure 10.- Typical acceleration-time histories for accelerations measured along the Z-axis. All values are model scale.

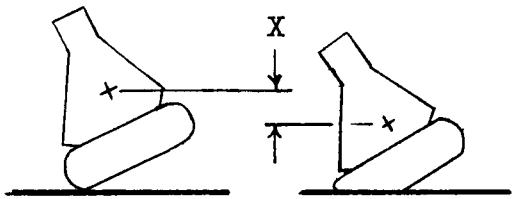

Flight path	Contact attitude
90°	0°
90°	33°
62°	-6°
62°	33°
62°	-17°

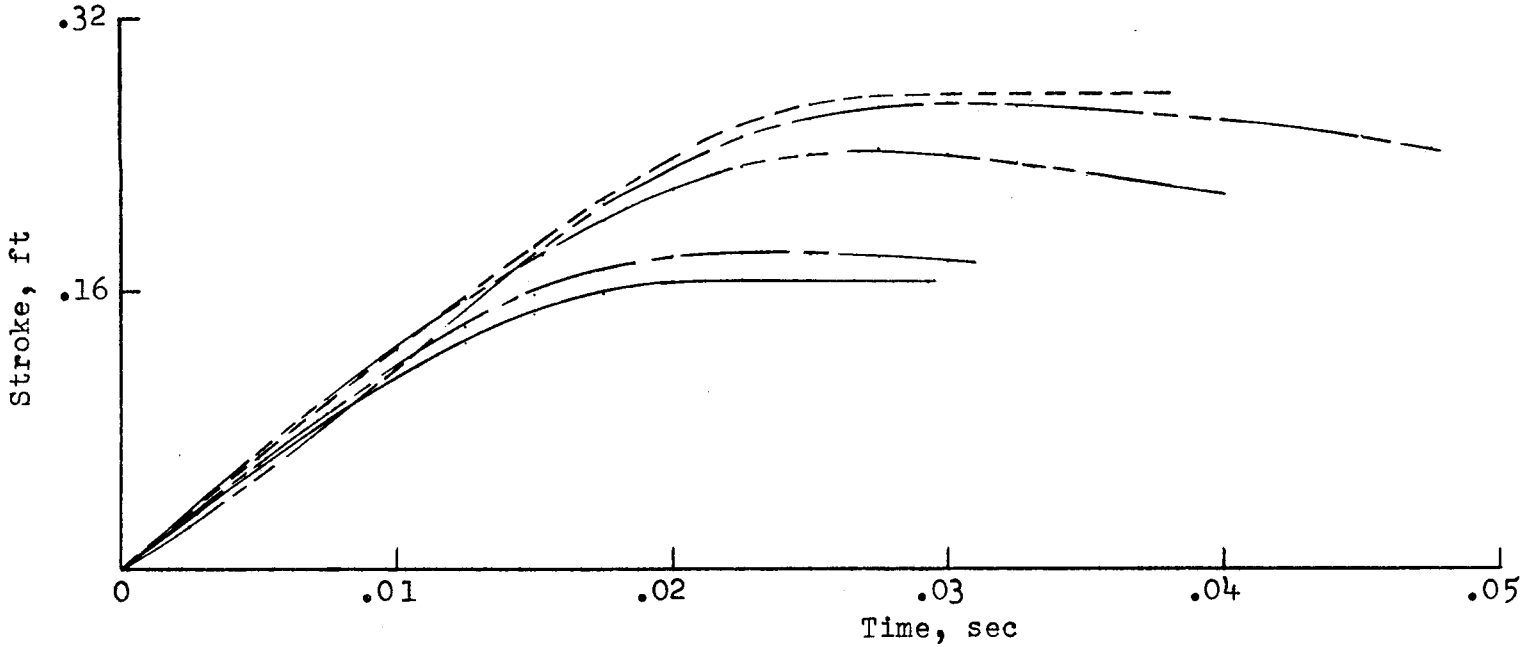

Figure 11.- Typical stroke-time histories. All values are model scale.

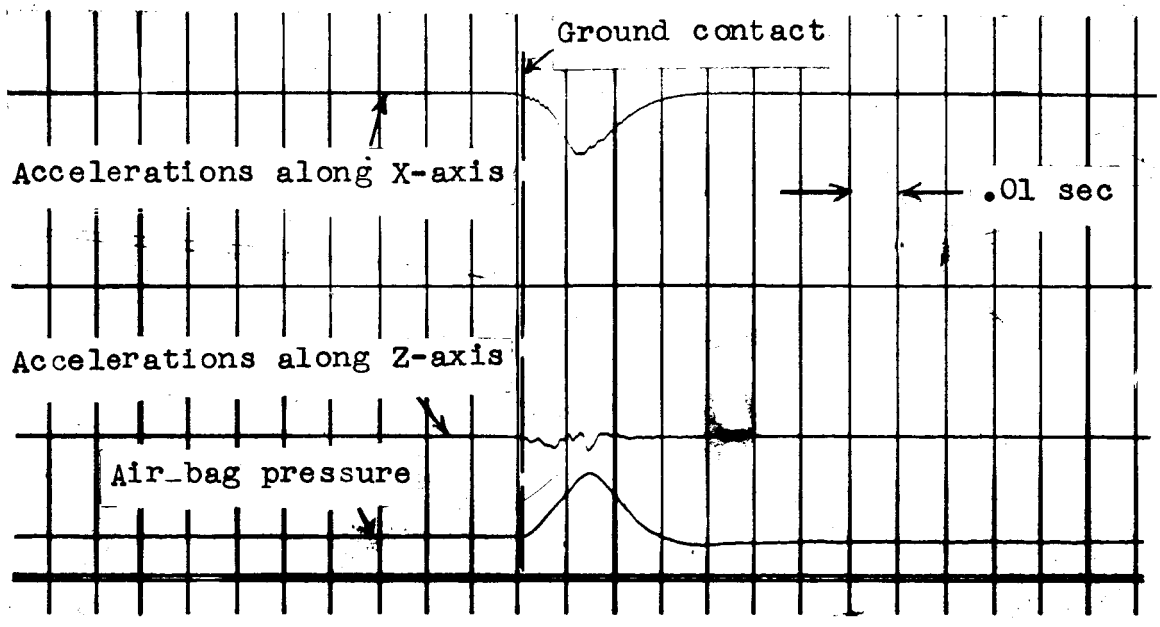

(a) Flight path, 90°; contact attitude, 0°.

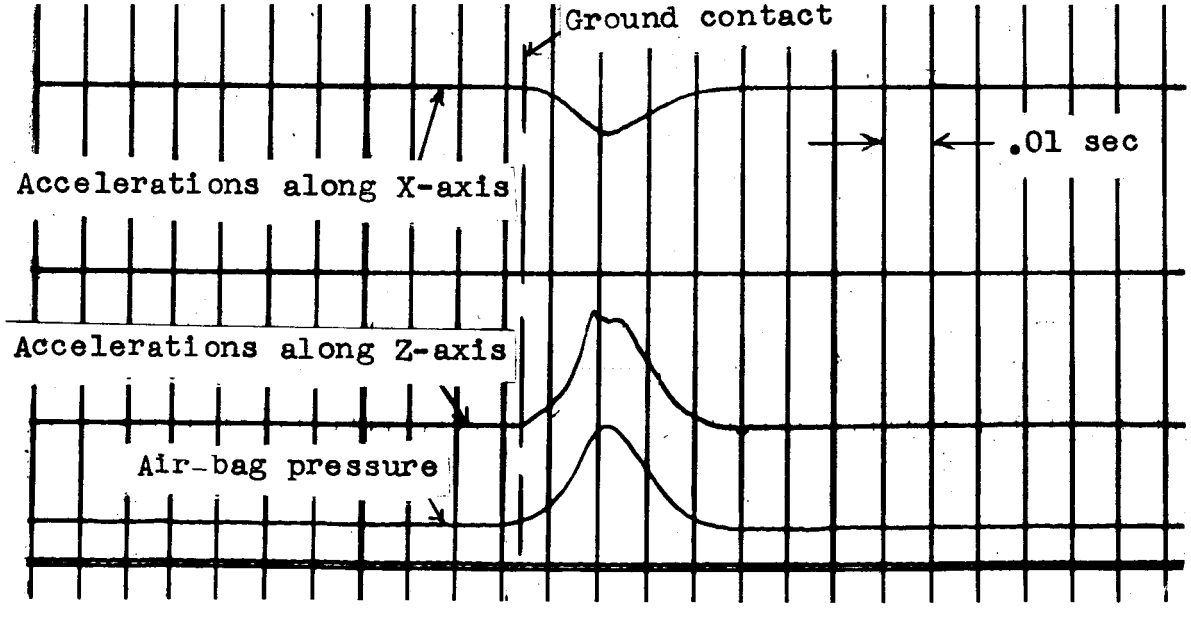

(b) Flight path, 62°; contact attitude, 33°.

Figure 12.- Typical oscillograph records of accelerations and air-bag pressure.

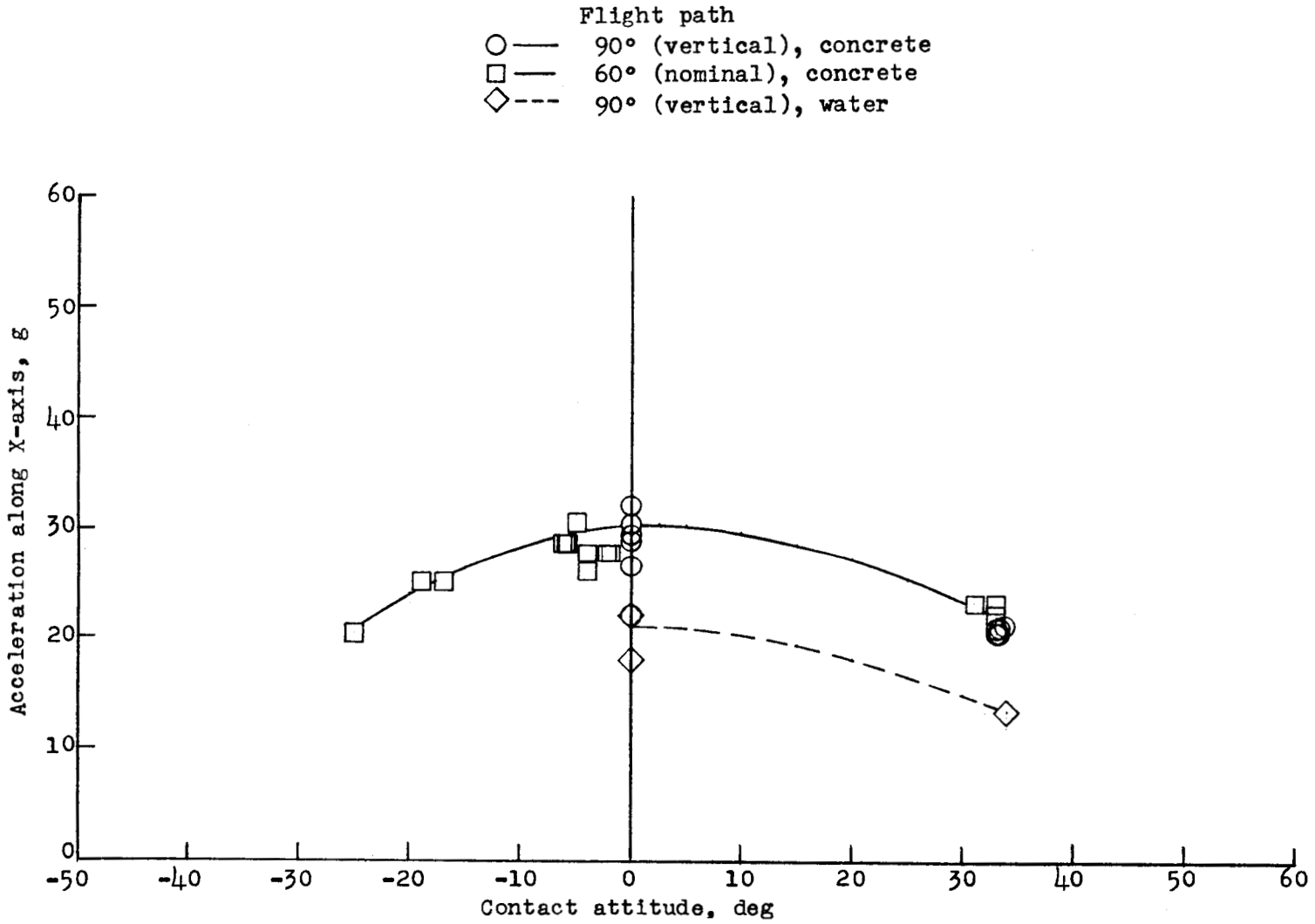

Figure 13.- Acceleration along X-axis as a function of contact attitude for landings on concrete and water.

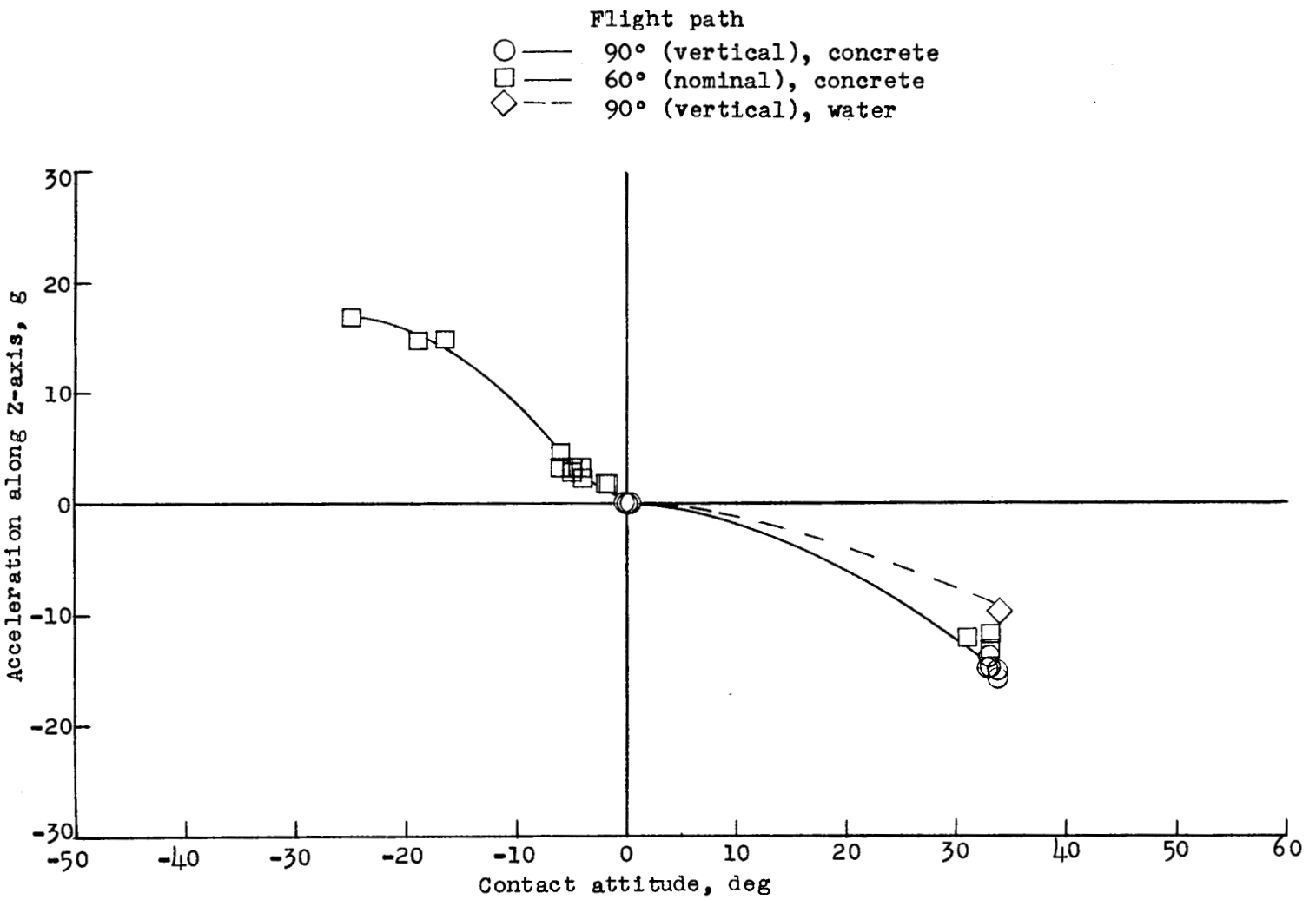

Figure 14.- Accelerations along Z-axis as a function of contact attitude for landings on concrete and water.

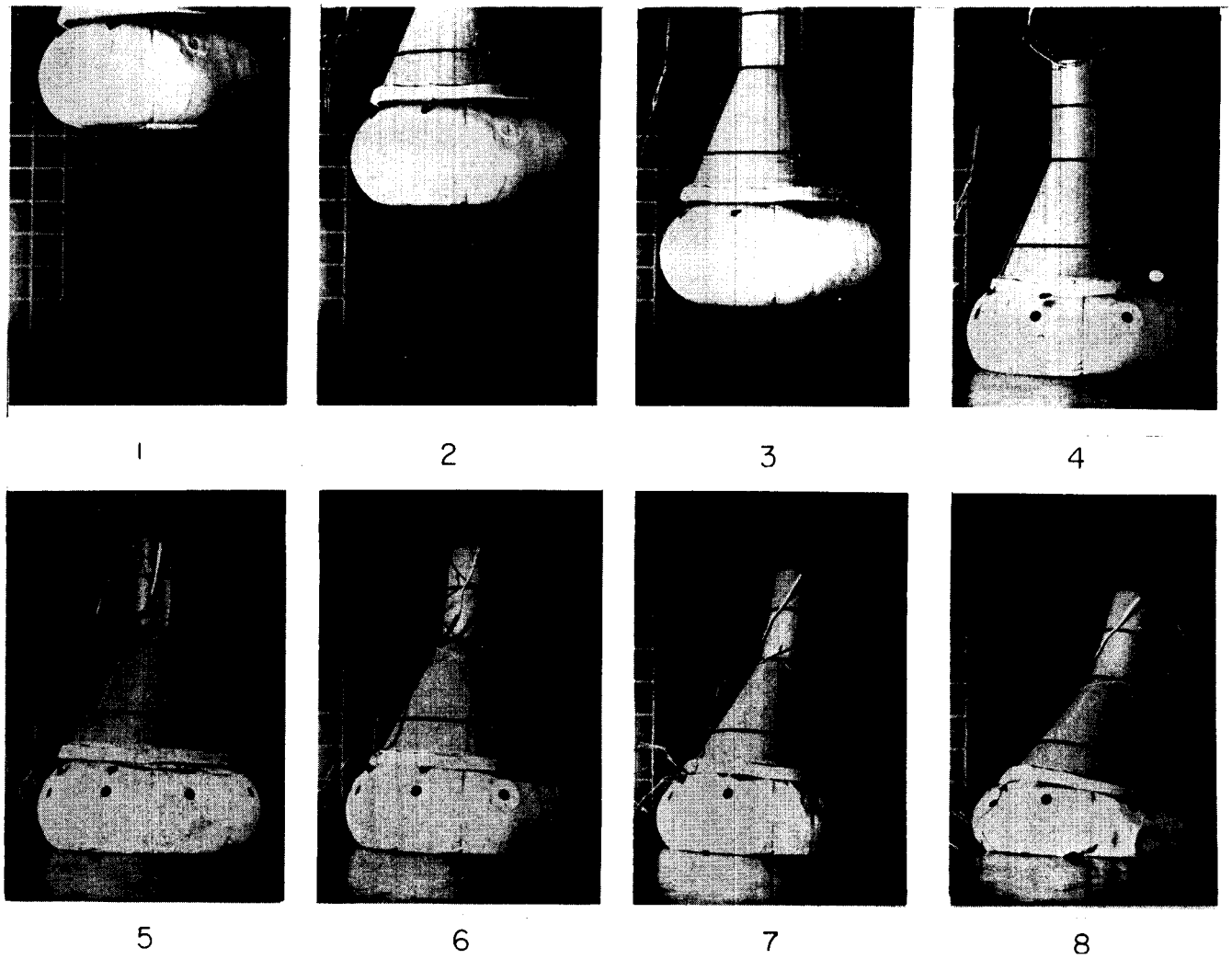

L-60-5543

Figure 15.- Sequence photographs of a test drop along a 90° (vertical) flight path for a 0° contact attitude.

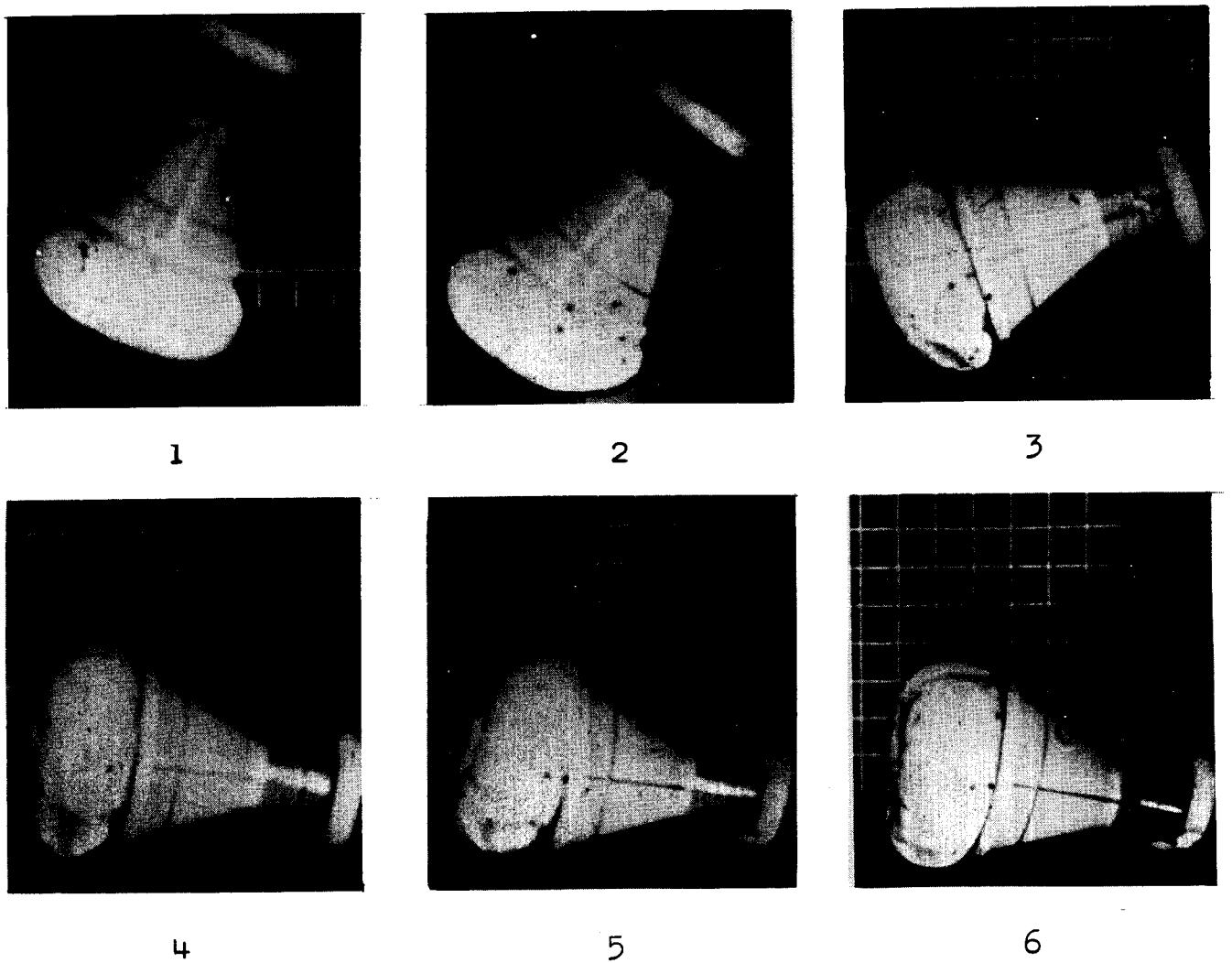

L-60-5544

Figure 16.- Sequence photographs of a test drop along a 63° flight path for a -26° contact attitude.

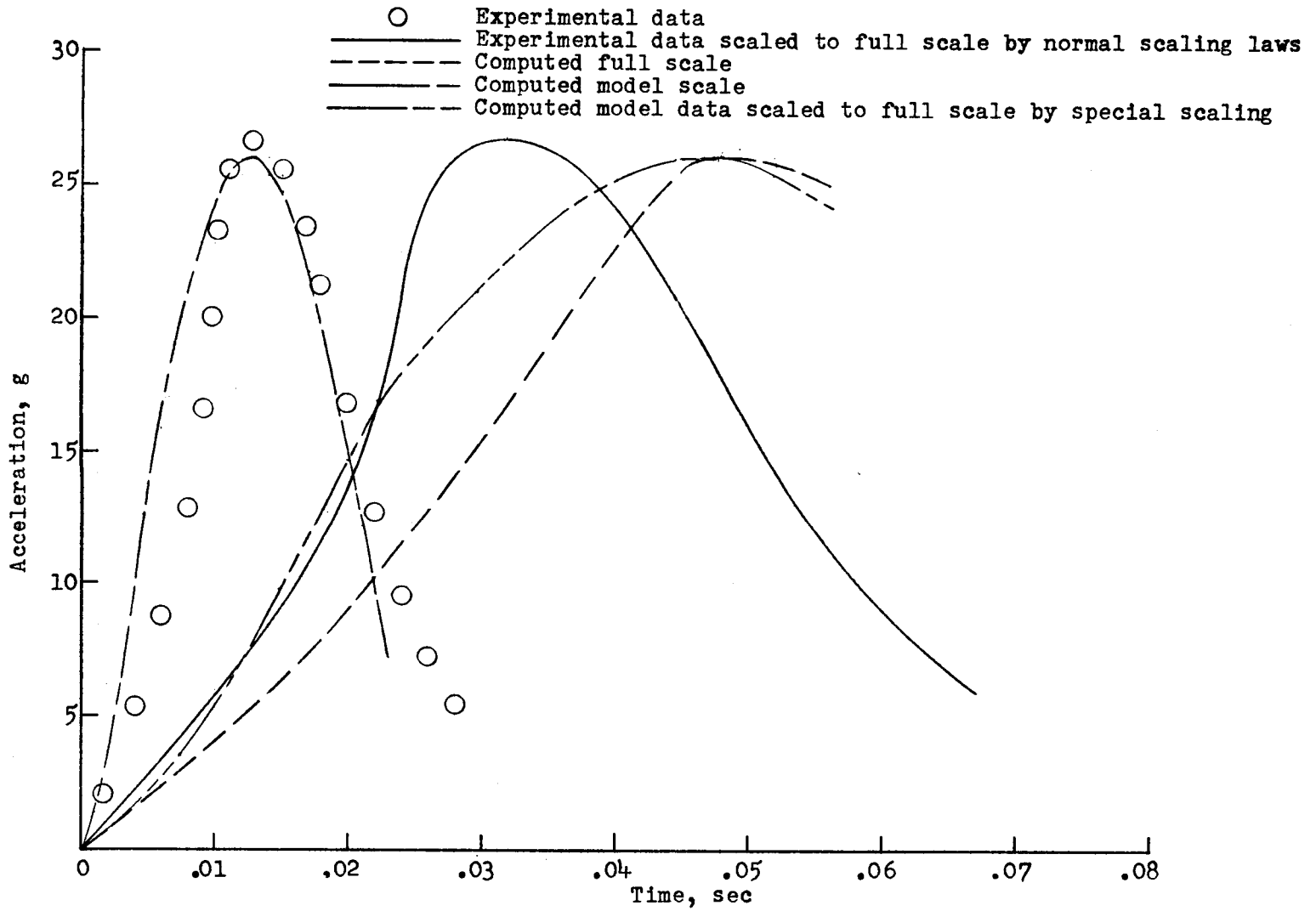

Figure 17.- Comparison of computed and experimental time histories of acceleration along the X-axis for a flight path of 90° (vertical) and a contact attitude of 0°.

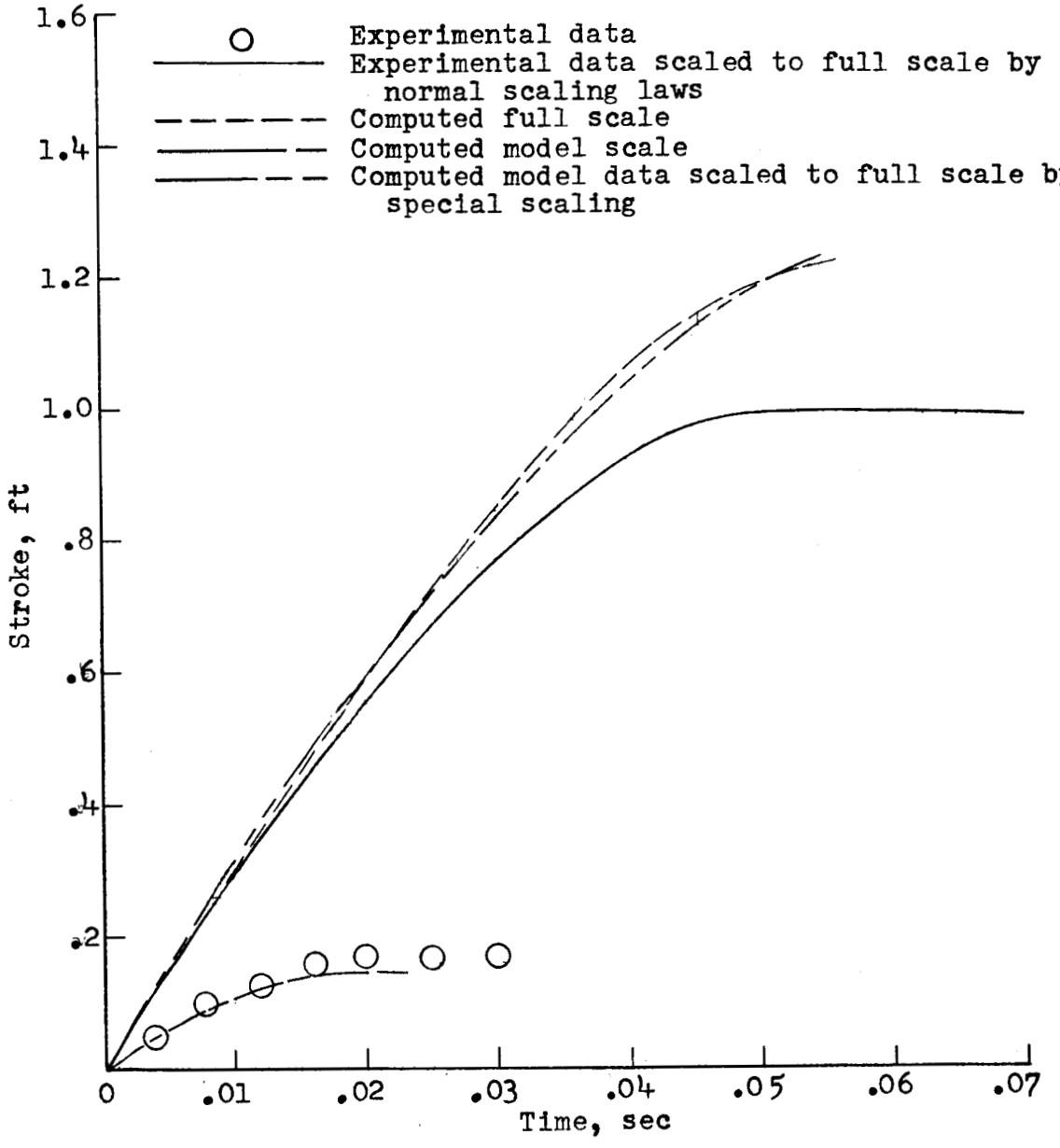

Figure 18.- Comparison of computed and experimental stroke-time histories for a flight path of 90° (vertical) and a contact attitude of 0°.

L-792